spires to possess magnetic properties common to both of the other carbon allotropes: it has a feeble diamagnetism, much like diamond (Fig. 1), but possesses ring currents, as in graphite. □

R. C. Haddon is at AT&T Laboratories, Murray Hill, New Jersey 07974-0636, USA.

1. Raman, C. V. *Nature* **123,** 945 (1929).
2. Ehrenfest, P. *Physica* **5,** 388–391 (1925).
3. Pauling, L. *J. chem. Phys.* **4,** 673–677 (1936).
4. Lonsdale, K. *Proc. R. Soc.* **159,** 149–161 (1937).
5. Van Vleck, J. H. *The Theory of Electric and Magnetic Susceptibilities* (Oxford Univ. Press, 1965).
6. Garratt, P. J. *Aromaticity* (Wiley, New York, 1986).
7. Minkin, V. I., Glukhovtsev, J. N. & Simkin, B. Y. *Aromaticity and Antiaromaticity* (Wiley, New York, 1994).
8. Kroto, H. W., Heath, J. R., O'Brien, S. C., Curl, R. F. & Smalley, R. E. *Nature* **318,** 162–164 (1985).
9. Smalley, R. E. *Chem. Engng News* **66(35),** 33–35, Aug. 29 (1988).
10. Elser, V. & Haddon, R. C. *Nature* **325,** 792–794 (1987).
11. Elser, V. & Haddon, R. C. *Phys. Rev.* A**36,** 4579–4584 (1987).
12. Haigh, C. W. & Mallion, R. B. *Prog. NMR Spectrosc.* **13,** 303–344 (1980).
13. Krätschmer, W., Lamb, L. D., Fostiropoulos, K. & Huffman, D. R. *Nature* **347,** 354–358 (1990).
14. Haddon, R. C. *et al. Nature* **350,** 46–47 (1991).
15. Ruoff, R. S. *et al. J. phys. Chem.* **95,** 3457–3459 (1991).
16. Hückel, E. *Z. Phys.* **70,** 204–286 (1931).
17. Hückel, E. *Z. Phys.* **60,** 423–456 (1930).
18. Haddon, R. C. *Acc. chem. Res.* **21,** 243–249 (1988).
19. Dauben, H. J., Wilson, J. D. & Laity, J. L. *J. Am. chem. Soc.* **91,** 1991–1998 (1969).
20. Haddon, R. C. & Elser, V. *Chem. Phys. Lett.* **169,** 362–364 (1990).
21. Schmaltz, T. G. *Chem. Phys. Lett.* **175,** 3–5 (1990).
22. Popie, J. A. *J. chem. Phys.* **24,** 1111 (1956).
23. Pasquarello, A., Schluter, M. & Haddon, R. C. *Science* **257,** 1660–1661 (1992).
24. Pasquarello, A., Schluter, M. & Haddon, R. C. *Phys. Rev.* A**47,** 1783–1789 (1993).
25. Suzuki, T., Li. Q., Khemani, K. C. & Wudl, F. *J. Am. chem. Soc.* **114,** 7301–7302 (1992).
26. Prato, M., Suzuki, T., Wudl, F., Lucchini, V. & Maggini, M. *J. Am. chem. Soc.* **115,** 7876–7877 (1993).
27. Prato, M. *et al. J. Am. chem. Soc.* **115,** 8479–8480 (1993).
28. Isaacs, L., Wehrsig, A. & Diederich, F. *Helv. chim. Acta* **76,** 1231–1250 (1993).
29. Smith, A. B. *et al. J. chem. Soc., chem. Commun.* 2187–2188 (1994).
30. Wudl, F. *Acc. Chem. Res.* **25,** 157–161 (1992).
31. Haddon, R. C. *Science* **261,** 1545–1550 (1993).
32. Taylor, R. & Walton, D. R. M. *Nature* **363,** 685–693 (1993).
33. Saunders, M. *et al. Nature* **367,** 256–258 (1994).
34. Haddon, R. C. *Nature* **367,** 214 (1994).
35. Cioslowski, J. *J. Am. chem. Soc.* **116,** 3619–3620 (1994).
36. Cioslowski, J. *Chem. Phys. Lett.* **227,** 361–364 (1994).
37. Bühl, M. *et al. J. Am. chem. Soc.* **116,** 6005–6006 (1994).
38. Haddon, R. C. & Pasquarello, A. *Phys. Rev.* B**50,** 16459–16463 (1994).
39. Bühl, M. & Thiel, W. *Chem. Phys. Lett.* **233,** 585–589 (1995).
40. Fowler, P. W., Lazzeretti, P. & Zanasi, R. *Chem. Phys. Lett.* **165,** 79–86 (1990).
41. McWeeny, R. *Molec. Phys.* **1,** 311–321 (1958).
42. Mallion, R. B. *Molec. Phys.* **25,** 1415–1432 (1973).
43. Mallion, R. B. *J. chem. Phys.* **75,** 793–797 (1981).
44. Haddon, R. C. *Tetrahedron* **28,** 3613–3634, 3635–3655 (1972).
45. Zanasi, R. & Fowler, P. W. *Chem. Phys. Lett.* **238,** 270–280 (1995).
46. Heremans, J., Olk, C. H. & Morelli, D. T. *Phys. Rev.* B**49,** 15122–15125 (1994).
47. Luo, W., Wang, H., Ruoff, R. S., Cioslowski, J. & Phelps, S. *Phys. Rev. Lett.* **73,** 186–188 (1994).
48. Ramirez, A. P. *et al. Science* **265,** 84–86 (1994).
49. David, W. I. F. *et al. Nature* **353,** 147–149 (1991).
50. Saunders, M. *et al. J. Am. chem. Soc.* **117,** 9305–9308 (1995).
51. Bausch, J. W. *et al. J. Am. chem. Soc.* **113,** 3205–3206 (1991).
52. van Ruitenbeek, J. M. & van Leeuwen, D. A. *Phys. Rev. Lett.* **67,** 640–643 (1991).
53. McClure, J. W. *Phys. Rev.* **104,** 666–671 (1956).
54. McClure, J. W. *J. chim. Phys.* **57,** 859–865 (1960).
55. Hoarau, J. & Volpilhac, G. *Phys. Rev.* B**14,** 4045–4053 (1976).
56. Volpilhac, G. & Hoarau, J. *Phys. Rev.* B**17,** 1445–1449 (1978).
57. Iijima, S. *Nature* **354,** 56–58 (1991).
58. Ebbesen, T. W. & Ajayan, P. M. *Nature* **358,** 220–222 (1992).
59. Lu, J. P. *Phys. Rev. Lett.* **74,** 1123–1126 (1995).
60. Wang, X. K., Chang, R. P. H., Patashinski, A. & Ketterson, J. B. *J. Mater. Res.* **9,** 1578–1582 (1994).
61. Chauvet, O. *et al. Phys. Rev. B* (in the press).
62. London, F. *J. Phys. Radium, Paris* **8,** 397–409 (1937).
63. Fleischer, U., Kutzelnigg, W., Lazzeretti, P. & Mülenkamp, V. *J. Am. chem. Soc.* **116,** 5298–5306 (1994).

ACKNOWLEDGEMENTS. I thank V. Elser, A. Pasquarello, A. P. Ramirez and the late M. A. Schlueter for their contributions to this work.

LETTERS TO NATURE

Evidence for shock acceleration of high-energy electrons in the supernova remnant SN1006

K. Koyama*, R. Petre†, E. V. Gotthelf†‡, U. Hwang†, M. Matsuura§, M. Ozaki* & S. S. Holt†

* Department of Physics, Kyoto University, Sakyo-ku, Kyoto 666-01, Japan
† Laboratory for High Energy Astrophysics, NASA/GSFC, Greenbelt, Maryland 20771, USA
‡ Universities Space Research Association, 7501 Forbes Blvd, Seabrook, Maryland 20706, USA
§ Department of Physics, Kyoto Sangyou University, Kita-ku, Kyoto 603, Japan

HIGH-ENERGY cosmic rays (relativistic heavy nuclei) play an important role in heating interstellar matter in the Milky Way[1,2], and they affect chemical abundances through collisions with atoms in the interstellar gas[2]. Although it has long been thought that these cosmic rays arise from supernovae[3,4], direct evidence for such an association has been lacking. Here we report X-ray observations of the remnant of supernova 1006, made by the ASCA satellite, which indicate that emission from the edges of the remnant shell is dominated by radiation from electrons accelerated to energies of ~100 TeV within the shock front. Ions in the shell are likely to have been accelerated to similar energies, thus giving rise to very-high-energy cosmic rays.

The X-ray CCD cameras on the ASCA observatory (the Solid-state Imaging Spectrometers) offer unprecedented capability for carrying out spatially resolved X-ray spectroscopy, with a broad bandpass (0.5–10 keV) and good spectral (~100 eV at 1 keV) and spatial (1 arcmin full width at half maximum) resolution[5]. Two 25-ks pointings were performed at the ~30-arcmin-diameter supernova remnant SN1006 with the 22 × 22 arcmin field of view CCD instruments: one centred on the remnant and the other on the northeastern rim. Figure 1 shows a mosaic 0.4–8.0 keV image of SN1006. As with the previous observations[6,7], we observe a shell-like structure, dominated by the northeastern (NE) and southwestern (SW) rims, whose surface brightness is an order of magnitude higher than in the other regions. The limb-brightened X-ray morphology is typical of supernova remnants (SNR) dominated by thermal processes in the shock-heated interstellar material and/or supernova ejecta.

Figure 2 shows X-ray spectra from regions along the bright NE rim (Fig. 2*a*) and near the (projected) centre of the remnant (Fig. 2*b*). The spectrum of the rim (Fig. 2*a*) is virtually featureless. The overall 0.4–8.0 keV spectrum is well fitted ($\chi^2 = 344$, with 332 degrees of freedom) by a model consisting of a power law with energy spectral index $\alpha = 1.95 \pm 0.20$, and two emission lines (K-shell resonance transitions of He-like and H-like O at 574 eV and 653 eV). Substitution of a thermal Bremsstrahlung model for the power law yields an unacceptable fit ($\chi^2 = 930$). As the bright rims are responsible for ~75% of the X-ray flux from SN1006 above 1 keV, this is the integrated spectrum measured by previous detectors lacking spatial resolution[8–11]. The best-fit energy spectral index found by ASCA is steeper than the $\alpha = 1.2$ inferred from the earliest observations[8], but consistent with the most sensitive observations[11]. It is also steeper than the $\alpha \approx 1.0$ characteristic of the Crab Nebula and similar SNR, whose centrally concentrated X-ray emission arises from synchrotron radiation produced by electrons accelerated to high energy in the pulsar magnetosphere[12]. The featureless spectrum from SN1006 is a

long-standing mystery. The X-ray spectra of all other young SNR with shell-like morphologies (for example, Cassiopeia A[13–15], Tycho[14,16] and Kepler[17]) are dominated by emission lines characteristic of shock-heated, optically thin plasma.

The important new information about SN1006 provided by ASCA is the spectral character of the remainder of the SNR. As shown in Fig. 2*b*, the spectrum of the interior contrasts sharply with that of the northwestern (NE) rim. It is dominated by emission lines characteristic of highly ionized elements, like the X-ray spectra of other young SNR. To our knowledge, this is the first detection of X-ray emission lines other than oxygen[18,19] from SN1006, and their presence is highly suggestive of an origin in a hot plasma. The spectrum has been fitted using time-dependent ionization models from the hydrodynamic simulation codes (also known as non-equilibrium ionization models) of Hughes and Helfand[20] and Hamilton *et al.*[21]. The best-fit model ($\chi^2 = 251$, with 235 degrees of freedom), has an emission-weighted electron temperature of 1.8×10^7 K, and ionization timescale $nt \approx 300$ cm^{-3} yr (where n and t are the electron density and elapsed time after the plasma was shock-heated to temperature kT). Although near-solar abundances of O, Ne and Fe are required, the Si abundance is at least an order of magnitude in excess of the solar value, and Mg and S relative abundances comparable to Si are allowed. The relative abundances are consistent with the calculated nucleosynthesis yields for type Ia supernovae (a supernova caused by accretion-induced ignition of a white dwarf, as opposed to core collapse of a massive star)[22]. The relatively low iron abundance is also consistent, as ultraviolet absorption line measurements show iron concentrated interior to the reverse shock and therefore not yet highly ionized[23–25]. A contribution from a hard, featureless component is required to obtain acceptable fits above 2 keV. The low nt value implies that the plasma is at least as far from ionization equilibrium as the younger remnants Tycho and Kepler[26]. We found no evidence for strong spatial variation of the spectrum with radius inside the shell or along the northwestern rim; that is, the spectrum shown in Fig. 2*b* is representative of everywhere in the remnant *except* the bright NE and SW rims. Also, the surface brightness of the oxygen lines is approximately the same at the rims as in the interior. This suggests that thermal emission pervades SN1006, but is dominated by a second, featureless component along the two rims.

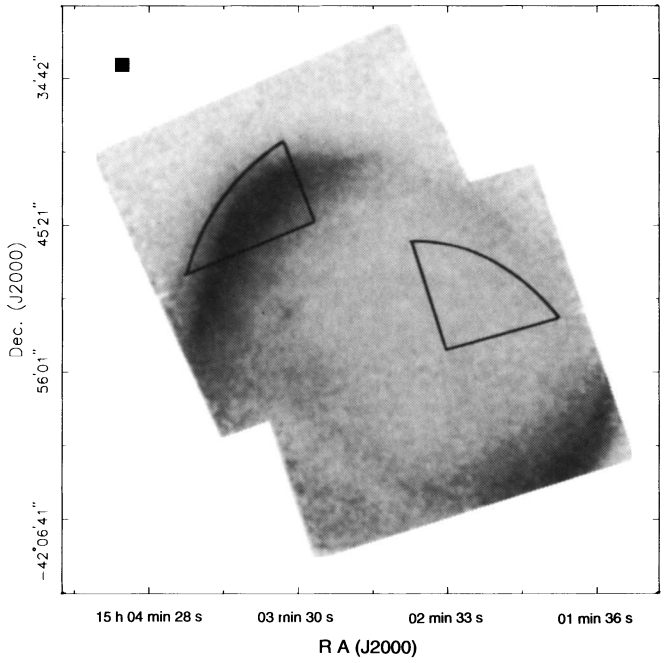

FIG. 1 CCD (charge-coupled-device) image of SN1006 in the 0.4–8 keV band, from the ASCA satellite. This image is an exposure-corrected mosaic of two pointings, one centred on the SNR and the other on the NE rim. The 'boxes' indicate the regions from which the spectra displayed in Fig. 2 were extracted. The odd shapes result from restricting the extraction to events from single CCD chips from the 4-CCD mosaicing comprising the Solid-state Imaging Spectrometer array for reduction of calibration uncertainties. The filled rectangle at the upper left is ~1 arcmin on a side.

Although previous measurements, most notably using the Imaging Proportional Counter on the Einstein satellite[6], indicated strong spectral differences between the bright rims and elsewhere in the remnant, the ASCA data dramatically reveal the different character of the spectra from the two regions. Rosat High Resolution Imager observations reveal that in addition to this spectral difference there is a morphological difference: only for the bright segments is there a strong correlation between X-ray and radio surface brightness[7].

Previous modelling efforts have focused on explaining the featureless continuum which dominates the integrated spectrum of SN1006 above 1 keV (refs 27–30). The generally accepted interpretation has been a shocked plasma under extreme non-equilibrium ionization conditions. This model, developed by Hamilton *et al.*[28,29], is based on a one-dimensional simulation of layered ejecta propagating into a uniform interstellar medium (ISM), wherein the X-ray emission arises primarily from reverse-shocked ejecta. Bremsstrahlung emission from fully ionized carbon in the outer ejecta layer gives rise to a power-law continuum X-ray spectrum with $\alpha = 1$ in this model. The extreme weakness (that is, absence) of the X-ray lines compared with SNRs like Tycho is simply a consequence of a weaker reverse shock propagating into the ejecta, which in turn is due to expansion of the forward shock into a substantially lower-ambient-density medium. As a result, the layer containing the intermediate-mass ejecta (Mg, Si, S) has not yet become sufficiently ionized to produce copious X-ray line emission.

The model of Hamilton *et al.*[28,29], which assumes that the spectrum is everywhere the same, cannot account for the observed spectral variations in SN1006, nor can it account for the revised value of α. The spectral differences along the rim require an azimuthal asymmetry in either the ISM or the ejecta, whereas a spectral index steeper than unity requires that the initial density of either the ISM or the outer ejecta of ionized carbon depends on the distance from the explosion centre. Whereas the spatial uniformity of the line emission suggests that oxygen and the intermediate-mass elements (Mg and Si in particular) are symmetrically distributed, the strong featureless continuum requires the fully ionized carbon to be concentrated in the bright rims. As C and O are intimately related in nucleosynthesis processes, no supernova model predicts different spatial distributions for these elements. Additionally, the strengths of the lines from the intermediate-mass elements, which arise deep within the ejecta layer, require a stronger reverse shock (and thus a generally denser ISM) than is allowed by the model of Hamilton *et al.* (the measured surface brightness of the Si line at 1.86 keV is a factor of five higher than predicted). Finally, as the volume emissivity of a thermal plasma is proportional to the square of the density, one would expect that the density of the X-ray-emitting plasma at the rims would be a factor of three higher than elsewhere from the relative surface brightness across the remnant. If this were so, then the line emission should be stronger relative to the continuum at the bright rims, and not weaker. These inconsistencies force us to conclude that in contrast with other young SNR, any thermal model attempting to describe SN1006 must be extremely complicated, requiring *ad hoc* assumptions about strong asymmetries in the ISM and possibly the ejecta.

A natural alternative is that the excess rim emission is intrinsically non-thermal[27,30], arising as synchrotron emission from electrons accelerated to relativistic energies within the shock region by the first-order Fermi mechanism[31]. This additional

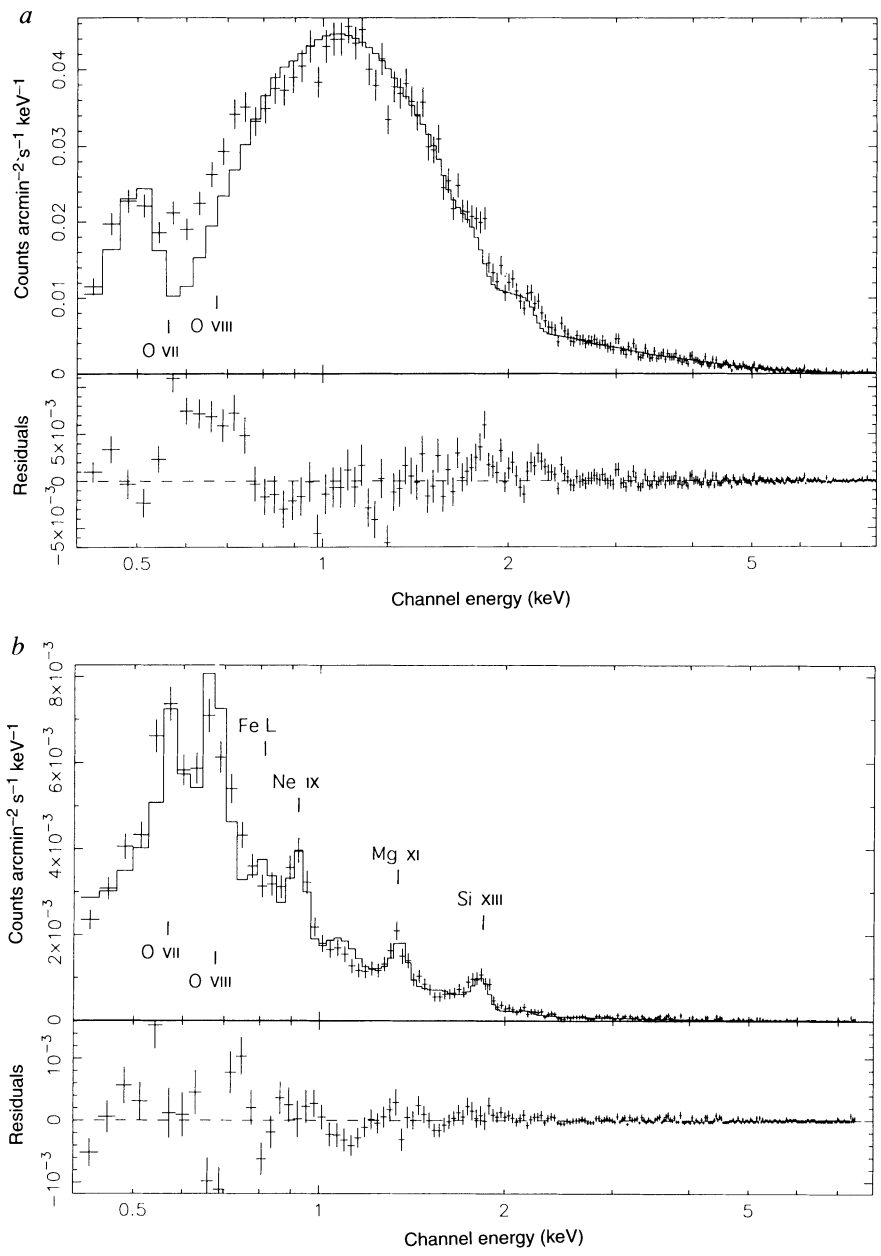

FIG. 2 Spectrum of the bright NE rim of SN1006. The best-fit model consists of a power law with energy spectral index $\alpha = 1.95 \pm 0.20$, two narrow O lines at 0.574 keV and 0.653 keV, and a column density slightly in excess of Galactic ($N_H = 1.8 \times 10^{21}$ cm^{-2}). The solid line superposed on the data is the power-law model, without the O lines. The O lines appear blended in the plot of the residuals. *b*, Spectrum of the interior of SN1006. Narrow emission lines, as marked on the figure, are detected at energies of 0.574, 0.653, 0.915, 1.34 and 1.86 keV, corresponding to the K-shell resonance transitions of He- and H-like oxygen, and He-like Ne, Mg and S, respectively. The line at 0.84 keV corresponds to an L-shell transition of Fe. The solid curve represents the best-fit non-equilibrium ionization model plus a hard component.

component is superposed on a thermal spectrum resembling that of other young SNR, which can be described within the framework of the Hamilton *et al.* model[28,29]. The synchrotron origin of the excess emission is supported by the strong correlation between the radio and X-ray surface brightness along the NE rim, in contrast to the lack of correlation along the thermal NW rim[18]. Published models of this process reproduce the flat radio spectrum and the steeper X-ray spectrum by predicting a power-law spectrum whose slope breaks between the radio and X-ray bands as synchrotron losses become important[27,30]. Although these models do not accurately produce the surface brightness correlation, more recent work does so[32].

The implications of non-thermal X-ray emission associated with a supernova remnant shock are important. The energy of a synchrotron photon E_p is related to the electron energy E_e and the magnetic field B by:

$$E_p \approx 4\ \text{keV} \times (B/1\ \text{mG}) \times (E_e/10\ \text{TeV})^2$$

There is no measurement of the magnetic field strength for any type Ia SNR (of which SN1006 is thought to be an example[33,34]). The best estimate[35] is 6–10 μG. As the X-ray spectrum remains flat up to ~20 keV (refs 8, 11), we infer that electrons of energy $\geqslant$200 TeV are being produced in the SN1006 shock. These energies are among the highest inferred for electrons in any astrophysical setting.

More fundamentally, the potential identification of the SN1006 shell as a production site for such high-energy electrons provides the first strong observational evidence that very-high-energy cosmic rays are produced in SNR shocks. Theoretical treatments of particle acceleration via first-order Fermi processes do not draw distinctions between electrons and ions: highly relativistic particles ($E \gg m_p c^2$) of either charge are accelerated as the result of interaction with turbulence in the shock-compressed magnetic field[31]. Thus although the X-ray data provide direct evidence for the presence of very-high-energy electrons, there exists ample theoretical support for the presence of ions of similar energy—in other words, cosmic-ray nuclei. An energy of 200 TeV approaches the 'knee' of the cosmic-ray electron spectrum (~1,000 TeV), the energy at which it dramatically steepens. Our observations thus directly support for the first time the long-held assumption[36,37] that SNRs accelerate cosmic rays all the way up to the 'knee', and provides a means for discriminating

between competing models for the rate of energy gain during diffusive shock acceleration[36,37].

Although SN1006 is the only strongly supported example thus far of a SNR with non-thermal X-ray emission from the shell, there exist data suggesting this process occurs in other remnants as well. The next best example is Cas A, where the 4–8 keV continuum has an energy spectral index $\alpha = 1.7$ and a morphology highly correlated with that of the radio continuum, in sharp contrast with that of the X-ray line emission[15]. Other candidates are IC443, whose hard (5–20 keV) X-ray component can be fitted by a power law with $\alpha \approx 2$, and Tycho, for which theoretical estimates suggest that the continuum above ~4 keV might be dominated by non-thermal emission[30]. Careful spatially resolved X-ray spectroscopic studies of these and other remnants must be carried out before the prevalence of cosmic-ray acceleration in SNR shocks can be assessed. □

Received 28 July; accepted 5 October 1995.

1. Berezinskii, V. S., Bulanov, S. V., Dogiel, V. A., Ginzburg, G. L. & Ptuskin, V. S. *Astrophysics of Cosmic Rays* (North Holland, Amsterdam, 1990).
2. Wefel, J. P. in *Cosmic Rays, Supernovae and the Interstellar Medium* (eds Shapiro, M. M., Silberburg, R. & Wefel, J. P.) 29–55 (Kluwer, Dordrecht, 1991).
3. Shklovskii, I. S. *Dokl. Akad. Nauk SSSR* **91,** 475–478 (1953).
4. Ginzburg, V. L. *Dokl. Akad. Nauk SSSR* **92,** 1133–1136 (1953).
5. Tanaka, Y., Inoue, H. & Holt, S. S. *Publs astr. Soc. Japan* **46,** L37–L41 (1994).
6. Pye, J. P. *et al. Mon. Not. R. astr. Soc.* **194,** 569–582 (1982).
7. Winkler, P. F. & Long, K. S. in *The Soft X-Ray Cosmos* (eds Schlegel, E. M. & Petre, R.) 312–314 (Am. Inst. Phys., New York, 1994).
8. Becker, R. H., Szymkowiak, A. E., Boldt, E. A., Holt, S. S. & Serlemitsos, P. J. *Astrophys. J.* **240,** L33–L35 (1980).
9. Koyama, K., Szymkowiak, A. E., Boldt, E. A., Holt, S. S. & Serlemitsos, P. J. *Publs astr. Soc. Japan* **39,** 437–445 (1987).
10. Leahy, D. A., Nousek, J. & Hamilton, A. J. S. *Astrophys. J.* **374,** 218–226 (1991).
11. Ozaki, M., Koyama, K., Ueno, S. & Yamauchi, S. *Publs astr. Soc. Japan* **46,** 367–373 (1994).
12. Asaoka, I. & Koyama, K. *Publs astr. Soc. Japan* **42,** 625–632 (1990).
13. Becker, R. H. *et al. Astrophys. J.* **234,** L73–L76 (1979).
14. Petre, R. *et al.* in *UV and X-Ray Spectroscopy of Laboratory and Astrophysical Plasmas* (eds Silver, E. & Kahn, S.) 424–433 (Cambridge Univ. Press, 1993).
15. Holt, S. S., Gotthelf, E. V., Tsunemi, H. & Negoro, H. *Publs astr. Soc. Japan* **46,** L151–L155 (1994).
16. Becker, R. H. *et al. Astrophys. J.* **235,** L5–L8 (1980).
17. Becker, R. H., White, N. E., Boldt, E. A., Holt, S. S. & Serlemitsos, P. J. *Astrophys. J.* **237,** L77–L79 (1980).
18. Galas, C. M. F., Venkatesan, D. & Garmire, G. P. *Astrophys. Lett.* **22,** 103–108 (1982).
19. Vartanian, M. H., Lum, K. S. K. & Ku, W.H.-M. *Astrophys. J.* **288,** L5–L9 (1985).
20. Hughes, J. P. & Helfand, D. J. *Astrophys. J.* **291,** 544–560 (1985).
21. Hamilton, A. J. S., Sarazin, C. L. & Chevalier, R. A. *Astrophys. J. Suppl. Ser.* **51,** 115–148 (1983).
22. Nomoto, K., Thielemann, F.-K. & Yokoi, K. *Astrophys. J.* **286,** 644–658 (1986).
23. Wu, C.-C., Leventhal, M., Sarazin, C. L. & Gull, T. R. *Astrophys. J.* **269,** L5–L8 (1983).
24. Fesen, R. A., Wu, C.-C., Leventhal, M. & Hamilton, A. J. S. *Astrophys. J.* **327,** 164–177 (1988).
25. Hamilton, A. J. S. & Fesen, R.A. *Astrophys. J.* **327,** 178–196 (1988).
26. Tsunemi, H. in *New Horizon of X-Ray Astronomy—First Results from ASCA* (eds Makino, F. & Ohashi, T.) 81–93 (Universal Academy Press, Tokyo, 1994).
27. Reynolds, S. P. & Chevalier, R. A. *Astrophys. J.* **245,** 912–919 (1981).
28. Hamilton, A. J. S., Sarazin, C. L., Szymkowiak, A. E. & Vartanian, M. H. *Astrophys. J.* **297,** L5–L9 (1985).
29. Hamilton, A. J. S., Sarazin, C. L. & Szymkowiak, A. E. *Astrophys. J.* **300,** 698–712 (1986).
30. Ammosov, A. E., Ksenofontov, L. T., Nikolaev, V. S. & Petukov, S. I. *Astr. Lett.* **20,** 157–162 (1994).
31. Blandford, R. D. & Eichler, D. *Phys. Rep.* **154,** 1–74 (1987).
32. Reynolds, S. P. *Astrophys. J.* (submitted).
33. Minkowski, R. *Astr. J.* **71,** 371–373 (1966).
34. Stephenson, F. G., Clark, D. & Crawford, D. F. *Mon. Not. R. astr. Soc.* **180,** 567–584 (1977).
35. Reynolds, S. P. & Ellison, D. C. in *Proc. 22nd Int. Cosmic Ray Conf.* Vol. 2 404–407 (Dublin Inst. for Advanced Studies, Dublin, 1991).
36. Lagage, P. O. & Cesarsky, C. J. *Astr. Astrophys.* **125,** 249–257 (1983).
37. Jokipii, R. J. *Astrophys. J.* **313,** 842–846 (1987).
38. Wang, Z. R., Asaoka, I., Hayakawa, S. & Koyama, K. *Publs astr. Soc. Japan* **42,** 303–308 (1992).

ACKNOWLEDGEMENTS. U.H. is a NAS/NRC Research Associate. We thank S. Reynolds for insightful discussions.

Quantum confinement and light emission in SiO_2/Si superlattices

Z. H. Lu, D. J. Lockwood & J.-M. Baribeau

Institute for Microstructural Sciences, National Research Council of Canada, Ottawa, Ontario K1A 0R6, Canada

PHOTONIC devices are becoming increasingly important in information and communication technologies. But attempts to integrate photonics with silicon-based microelectronics are hampered by the fact that silicon has an indirect band gap, which prevents efficient electron–photon energy conversion. Light-emitting silicon-based materials have been made using band-structure engineering of SiGe and SiC alloys and Si/Ge superlattices, and by exploiting quantum-confinement effects in nanoscale particles and crystallites[1–3]. The discovery[4,5] that silicon can be etched electrochemically into a highly porous form that emits light with a high quantum yield has opened up the latter approach to intensive study[6–12]. Here we report the fabrication, by molecular-beam epitaxy, of well-defined superlattices of silicon and SiO_2, which emit visible light through photoluminescence. We show that this light emission can be explained in terms of quantum confinement of electrons in the two-dimensional silicon layers. These superlattice structures are robust and compatible with standard silicon technology.

The Si/SiO_2 superlattices were grown at room temperature on phosphorus-doped n-type (100) Si wafers by molecular-beam epitaxy in a VG Semicon V80 system. Thin Si films of various thickness were deposited on the ultraviolet/ozone-oxidized Si(100) wafer surface. A SiO_2 film ~1 nm thick was then grown *ex situ* by a rate-limited ultraviolet/ozone oxidation process. This procedure was repeated until a six-period Si/SiO_2 superlattice was made. The Si layer thickness and density were determined by small-angle X-ray scattering[13]. Modelling of the reflectivity profiles established the periodic nature of the structure and revealed the Si layers to be of the same high density as found in vacuum-deposited Si. This suggests that the concentration of hydrogen, if there is any, incorporated in the Si film during growth should be very low. The chemical modulation and high purity of the superlattices were confirmed by Ar^+-sputter profiling using Auger electron spectroscopy in a PHI 650 system. The physical structure of the superlattices was also studied by cross-sectional transmission electron microscopy (TEM) using a Philips EM 430 TEM operated at 300 kV. Figure 1 shows a cross-sectional TEM micrograph taken on a six-period SiO_2/Si superlattice with Si layer thickness of 2.8 nm and SiO_2

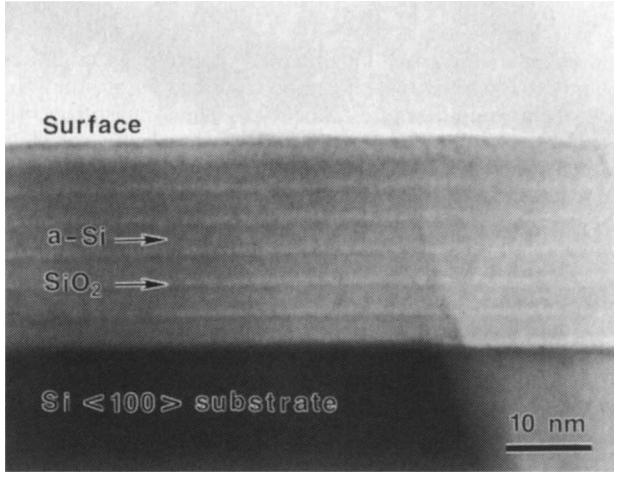

FIG. 1 Cross-sectional TEM micrograph taken from a six-period SiO_2/Si superlattice grown on Si(100) substrate. The alternating bright and dark bands represent SiO_2 and a-Si layers, respectively, as marked. The changes in the contrast on the right-hand side of the picture are caused by cleavage steps during TEM sample preparation.